Performance analysis of model-scale tidal stream turbines situated in different array configurations

*Matthew Allmark, **Stephanie Ordonez-Sanchez, ***Luke Myers, *Rob Ellis, *Catherine Lloyd, **Rodrigo Martinez, *Allan Mason-Jones, *Tim O'Doherty and **Cameron Johnston

***Abstract*—Tidal stream technology is a promising source of renewable energy which is expected to contribute to the global energy mix by 2050. The technology is currently still in its infancy and the road to commercialisation relies on extensive research and development that will improve the operability of tidal devices and increase the efficiency of power generation. This report presents the results of an experimental study into the performance of scale model horizontal axis tidal stream turbines placed in different array configurations.Optimising an array configuration can maximise power extraction which is essential in driving reductions in the levelised cost of energy associated with tidal power.**

In the experimental investigation presented, three scale model turbines were placed in four different configurations. The flow data and turbine performance data were analysed to determine which array generated the most favourable results. The four array layouts were all setup with two upstream devices with a single downstream device. These devices were set in a delta shape with tests repeated with differing lateral separation between upstream devices and longitudinal separation between the front row and the single downstream device. A single array configuration with the downstream device 7.8D downstream of the front row of turbines was tested along with three compact array cases with the downstream device was set at 3.2D downstream of the front row of devices. All three devices were operated at a constant rotational speed for a given test and array configuration as facilitated by the permanent magnet synchronous machine operating under servo control. To achieve a range of operating conditions for each array configuration, a range of experiments were undertaken at each layout with the downstream device operating at differing rotational velocities.

***Index Terms*—Enter at least three key words or phrases in alphabetical order, separated by commas.**

I. Introduction

THERE have been exciting developments in recent years which show promising signs that the sector is approaching commercialisation. The breakthrough project known as MeyGen is underway at the Pentland Firth, where the first 6 MW out of the proposed 398MW have been installed in phase 1A. The four 1.5 MW turbines have so far generated more than 17GWh of electricity to the grid [1]. Phase 1B will see the deployment of an additional 2 turbines as well as a sub-sea hub which will allow multiple turbines to be connected to a single power cable and thus reducing costs. Phase 1c involves the construction and deployment of 49 new turbines at an estimated cost of £420m. SIMEC Atlantis Energy believe that this will be a transformative phase for the industry as economies of scale come into play with increased production of turbines [2]. Currently the industry is at a cross roads where in order to reach commercialisation the cost of turbine construction as well as the associated cost of deploying turbines need to be reduced in order for the technology to become economically viable. The road to commercialisation relies upon the continuation of research into improving turbine operability and array efficiency. Nova Innovation, who successfully delivered the first grid connected off-shore array of tidal turbines near the Shetlands in Scotland, have been awarded with two European grants projects to bring down the cost of tidal energy. The EnFAIT project has already reported a reduction in operational costs of 15% and are aiming for a 40% reduction by 2022. The second project called ELEMENT started in June 2019 with the aim of reducing the overall lifetime cost of TS energy by 17% [3]. With continued support and investment in TS research, the industry hope that soon in the future the technology will become economically viable and will one –day compete with other renewable technologies. As sector develops and moves towards commercialisation there is a requirement to understand in detail the ramifications of array layout on tidal farm power production. The research presented herein has been conducted to aid in meet this requirement through 1/15th scale testing of a three turbine array under a variety of configurations. This paper is organised as follows: the following section, Section II details a selection of the research undertaken into array operation, this is followed in Section III by detail of the experimental setup and methodology used in this work, we then present the results of the test campaign in Section IV and finally we close the paper with conclusions in Section V.

This paragraph of the first footnote will contain the ID number of your paper submission and the conference track where the paper was submitted. This work was supported in part by EPSRC (EP/N020782); the access was supported Wave energy Scotland and UKCMER Flex Award 24835798"

Corresponding Author: Matthew Allmark, Email: Allmarkmj1@cardiff.ac.uk. *Cardiff Marine Energy Group, Cardiff University, The Parad, Cardiff, CF24 3AA.

Department of Mechanical and Aerospace Engineering, University of Strathclyde, 75 Montrose St, Glasgow G1 1XJ; * Engineering, University of Southampton, Southampton Boldrewood Innovation Campus, Burgess Road, Southampton, SO16 7QF

II. Tidal Arrays

A challenge faced by tidal array developers is to find a balance between ensuring that turbines aren't spaced too closely so that performance is compromised, but also to maximise the use of a site by packing in an optimal number of turbines. As demonstrated in the Mycek et al [4] study, a flow field generated from one turbine will affect the performance of a second-generation turbine if placed too close behind the first. Second generation turbines are therefore placed in the spaces left in between the upstream row. An efficient array configuration not only requires enough distance between the first and second row of turbines, but also an effective lateral distance to separate turbines in each row. To this end there have been a number of research activities over recent years which seek to optimise array structure by coupling various optimisation routines with methods to characterise the structure of the flow deficit created by an upstream device, either by simulation (actuator disk, BEMT and line actuator representations are common) or by curve fitting - see [5] [6] [7] [8] [9] [10]. Such optimisation approaches are computationally inexpensive and have shown promising results that array efficiencies (ratio of total power generated to power generated by an equal number turbines each isolation) of up to 90 % could be achievable.

Numerous experimental campaigns have also been undertaken, in a study by Myers and Bahaj [11] actuator disks were used to simulate HATTs and several layouts were tested in a flume in order to understand the impact of different array spacing and to classify different configurations. An interesting discovery was made where it was demonstrated that flow could be accelerated between a pair of actuator disks. When placed in configuration with 1.5 diameters of lateral space, measured flow velocity between the disks showed an increase of 22% in kinetic energy in comparison to flow conditions. When a third disk was placed 3 diameters downstream in the accelerated area of flow, it resulted in a reduction in velocity deficit within the wakes of the upstream disks and the wakes were forced around the downstream disk. The velocity deficit of the wakes then extended far beyond what was measured as a single row array, forming a combined wake with that generated by the third disk which was stronger and wider. What this suggests is that a third-row array would require greater longitudinal spacing.This study demonstrates the ability to develop an array configuration that accelerates flow velocity which could enhance the power extraction capability of the second-row turbine. However, it also demonstrates the complexity of this configuration as it leads to a greater overall wake effect which could negatively impact power generation of a third-row turbine. To overcome this problem, this study suggests that longitudinal spacing could be increased between different rows, for example the distance between row two and three would increase. It must be noted however that studies such as these are conducted in simulated flow environments and therefore produce results that could be considered over simplified and idealised. In real-sea conditions the efficiency of any array configuration will be further impacted by site bathymetry, topography and the presence of turbulence and surface waves [11]. The effect of accelerated bypass flow and the associated power output increases in down stream devices has been observed in numerous other laboratory scale test campaigns, see [12] [13] [4]

More recently, Noble et al [14] undertook a $1/15^{th}$ Scale tests, similar to the those presented here with the addition of a comprehensive flow measurement campaign. The work utilized a range of array configurations to appraise the effect of two upstream devices on the inflow conditions of a third downstream device. The work presents results from 4 configurations presenting the flow field without any devices, with only upstream devices, only the downstream device and finally with the three turbine array installed. The array in this work consisted of the two front turbines 1 diameter (1D) upstream of the back turbine and a lateral separation of the front two devices of 1.5 diameters (1.5D) either side of the back turbine. This work showed that closely packing devices could result in increased power production of the back turbine due to the accelerated bypass flow. Indeed the work reports a 5.7% to 10.5% increase in power production from the downstream device accompanied by a 4.8% to 7.3% increase in thrust.

This work builds upon the work reviewed by studying, for the first time at $1/15^{th}$-scale, the effects of varying the upstream device separation on the power produced by a downstream turbine a) with a large downstream separation and b) with a small downstream separation. The next section details the methodology used to undertake such a study.

III. Methodology

Three lab-scale HATTs were used to investigate the effect of turbine array spacing within the FloWave Ocean Energy Research Facility at the University of Edinburgh. The experimental testing was undertaken utilising three 0.9 m diameter lab-scale HATTs which were place in various configurations to test the effects of lateral spacing of the front row of tidal devices.

A. Instrumented Model Scale Turbine

Cardiff Marine Energy Research Group (CMERG) designed and manufactured a 3-bladed, 1:15 scale Horizontal Axis Tidal Turbine (HATT) which has a rotor diameter of 0.9m and hub diameter of 0.13m [15], as shown in 1. The three blades were 384.5 mm in length and were designed based on the Wortmann FX63-137 aerofoil, as detailed by [15], as shown in Figure 1B. A summary of the optimum settings used for this specific HATT configuration can be found in I.

The HATT's used were all direct drive and utilised a Permanent Magnet Synchronous Machine (PMSM) for the turbine control and power take-off. Back to back

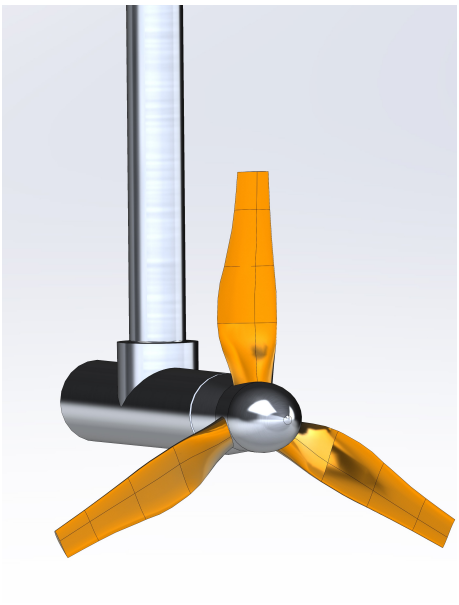

Fig. 1. The 0.9 m Horizontal Axis Tidal Turbine design utilised for this study,

TABLE I
ROTOR CHARACTERISTICS OF THE LAB SCALE HATT

Property	Value
No Blades	3
Blade Length	384.5 mm
Pitch Angle	6 ^{o}
Maximum Twist	19 ^{o}
Turbine Diameter	900 mm
Hub Diameter	130 mm

voltage source converters controlled the power flow to and from the motor, enabling both speed and torque control. Table II details the key design specifications used in developing the HATT.

B. Experimental Facility

Experimental testing was conducted at the FloWave Ocean Energy Research Facility at the University of Edinburgh, as shown in Figure 2. The FloWave facility is a unique, circular testing facility which can generate different combinations of waves and current in any relative direction across the central test volume. The combined wave and current circular tank has a diameter (D) of 25m, whereby its circumference is lined by 168 wavemaker paddles, as shown by (A) in Figure 3. Current re-circulation is driven across the test volume through turning vanes (B) by 28 impellers mounted below the test area (C), capable of achieving current

TABLE II
KEY DESIGN SPECIFICATIONS FOR THE LAB SCALE HATT

Specification	Details
Rated flow velocity	Continuous: 1.3 m/s Instantaneous: 1.5 m/s
Rated power	600 W
Rated torque	Continuous: 41 Nm Instantaneous 54 Nm
Rotational velocity	Rated: 350 RPM Maximum: 700 RPM
Maximum rotor thrust	1070 N

Fig. 2. The FloWave Ocean Energy Research Facility located at the University of Edinburgh, figure reproduced from [16].

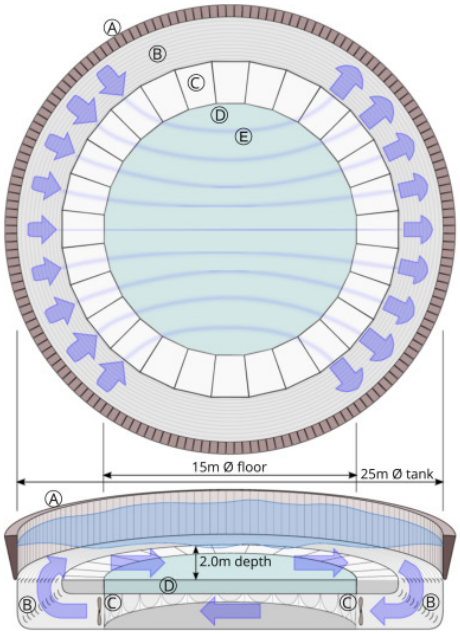

Fig. 3. A schematic drawing of the FloWave Ocean Energy Research Facility in plan and oblique section showing: (A) wavemaker paddles around circumference, (B) turning vanes and flow conditioning filters, (C) current drive impeller units, (D) buoyant raisable floor below test area, (E) idealised streamlines of flow across tank floor, figure reproduced from [16].

velocities ¿ 1.6 m/s [16]. Below the test area is a 15m diameter buoyant floor (D) which can be raised for turbine and instrumentation installation and then submerged to create a water depth of 2m [16].

C. Flow Measurement Techniques

The FloWave tank has an instrumentation gantry situated 1m above the water surface, as shown in Figures 4 and 5. An Acoustic Doppler Velocimeter (ADV) was attached to the gantry using an adjustable support and used to measure the flow velocity. The ADV used, A Nortek Vectrino Profiler, was a provided by the FloWave facility and calibrated by the manufacturer and was recorded at a sample rate of 100 Hz. The flow velocity was recorded 1D (0.9m) upstream of each turbine at the hub height (water depth = 1m) and measured the u, v and w velocities which correspond to the x, y and z directions. The tank was seeded with neutrally buoyant glass micro-spheres to produce and maintain $> 95\%$ mean correlation between beams [16] [14].

D. Experimental Procedure

Three lab-scale HATTs were placed into four different array configurations at the FloWave test facility,

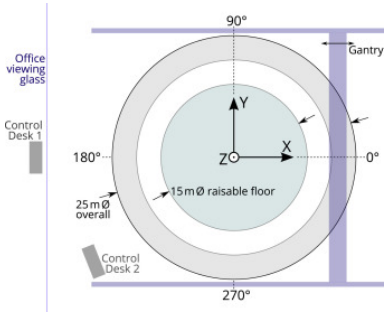

Fig. 4. The FloWave Ocean Energy Research Facility in plan view including the location of the instrumentation gantry and reference coordinate frame figure reproduced from [16].

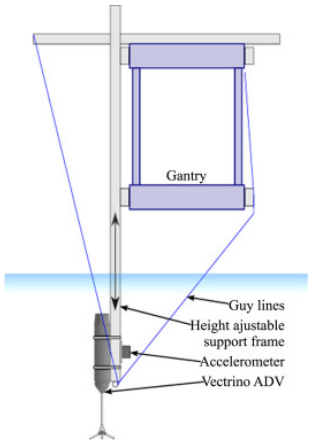

Fig. 5. The FloWave Ocean Energy Research Facility instrumentation set up schematic, figure reproduced from [16].

as illustrated in Figure 6. The lab-scale HATTs were mounted on a 0.87m stanchion which lead to a hub depth of 1m, centralised across the water column which had a water depth of 2m. The lateral distance between the two upstream turbines and the longitudinal distance between these and the downstream turbine was altered for each of the four array configurations, as illustrated by Figure 7 and detailed by Table III. In each array configuration, the inflow velocity was set to 0.95 m/s and the two upstream turbines were set to operate at peak power conditions which required a rotational speed of $\omega = 8.34 rads^{-1}$ equating to a Tip Speed Ratio (λ) of 4 as found in previous test campaigns [15] [12]. The downstream turbine was then tested over a range of rotational speeds as detailed in Table III.

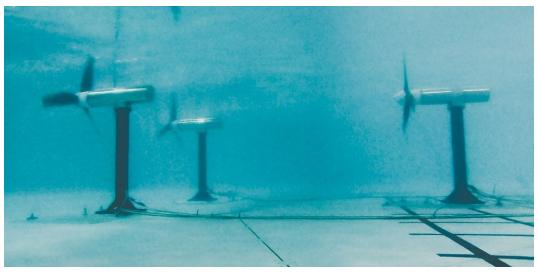

Fig. 6. An illustrative underwater photograph of one of the experimental array setups adopted.

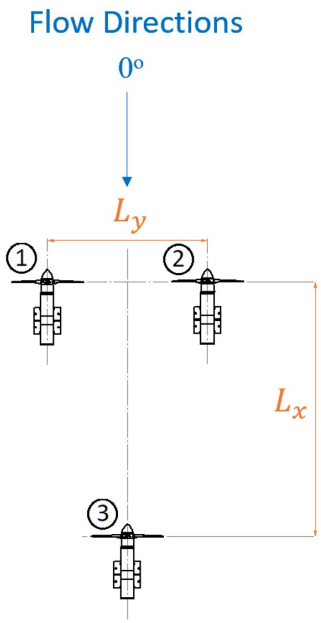

Fig. 7. A plan view schematic of the general array configurations with detail provided in Table III

TABLE III
OVERVIEW OF THE EXPERIMENTAL SETUPS TESTED IN RELATION TO FIGURE 7

	Setup 1	**Setup 2**	**Setup 3**	**Setup 4**
Inlet Vel U_∞ [m/s]	0.95	0.95	0.95	0.95
Lateral Spacing L_y [m]	1.80 (2.0D)	1.80 (2.0D)	2.40 (2.7D)	2.70 (3.0D)
Longitudinal spacing L_x [m]	7.07 (7.8D)	2.87 (3.2D)	2.87 (3.2D)	2.87 (3.2D)
Back Turbine Rotational Speeds, ω $[rads^{-1}]$	5.23 7.33 8.34 9.42 11.5	5.23 7.33 8.34 9.42 11.5	5.23 7.33 8.34 9.42 11.5	5.23 7.33 8.34 9.42 11.5

IV. RESULTS

A. Flow Measurement Analysis

This section presents the results of the flow measurements made upstream of each of the HATTs via the ADV instrumentation for each of the four cases studied. In all cases signals from the ADVs were firstly filtered to remove any spurious results or 'spikes' from the measured data, as are commonly found within such measurements. The filtering was achieved utilising a median filter set to the 5th order which offered a suitable compromise between over filtering and removing the majority of the spikes. Tables IV, V and VI provide an overview of the fluid statistics as captured with the ADV 1D upstream of the front left, front right and downstream devices, respectively. The statistics obtained suggest that the front of the array was on the very edge of the working section of the wave tank and in particular this was prominently observed in front of turbine 1 (front left) for which mean inflow angles of up to 6.16 degrees were observed with a large spread characterised by standard deviations of up to 11.57 degrees. There was an asymmetry in the resultant and stream-wise mean flow rates measured upstream of the front left and right devices, there is

TABLE IV
OVERVIEW OF THE FLUIDS STATISTICS 1D UPSTREAM OF THE TURBINE 1 (FRONT LEFT)

	Mean Flow Velocity X-Dir [m/s]	Mean Flow Velocity Y-Dir [m/s]	Mean Flow Velocity Z-Dir [m/s]	Mean Resultant Flow Velocity [m/s]	Turbulence Intensity [%]	Turbulent Kinetic Energy [J/kg]	Flow Angle α [^{o}]	Standard Deviation of Flow Angle α [^{o}]
Setup 1	0.88	0.09	-0.14	0.92	16.38	0.035	6.16	11.13
Setup 2	0.88	0.09	-0.14	0.92	15.16	0.029	5.88	9.54
Setup 3	0.83	0.07	-0.21	0.90	19.78	0.049	4.45	10.95
Setup 4	0.84	0.06	-0.18	0.89	18.25	0.041	3.71	11.57

TABLE V
OVERVIEW OF THE FLUIDS STATISTICS 1D UPSTREAM OF THE TURBINE 2 (FRONT RIGHT)

	Mean Flow Velocity X-Dir [m/s]	Mean Flow Velocity Y-Dir [m/s]	Mean Flow Velocity Z-Dir [m/s]	Mean Resultant Flow Velocity [m/s]	Turbulence Intensity [%]	Turbulent Kinetic Energy [J/kg]	Flow Angle α [^{o}]	Standard Deviation of Flow Angle α [^{o}]
Setup 1	0.95	-0.05	-0.09	0.96	8.23	0.009	-2.7	5.32
Setup 2	0.92	-0.04	-0.1	0.94	8.67	0.01	-2.48	5.69
Setup 3	0.98	-0.09	-0.07	0.99	4.99	0.004	-5.36	2.92
Setup 4	1.03	-0.1	-0.05	1.04	5.22	0.004	-5.64	3.05

TABLE VI
OVERVIEW OF THE FLUIDS STATISTICS 1D UPSTREAM OF THE TURBINE 3 (BACK)

	Mean Flow Velocity X-Dir [m/s]	Mean Flow Velocity Y-Dir [m/s]	Mean Flow Velocity Z-Dir [m/s]	Mean Resultant Flow Velocity [m/s]	Turbulence Intensity [%]	Turbulent Kinetic Energy [J/kg]	Flow Angle α [^{o}]	Standard Deviation of Flow Angle α [^{o}]
Setup 1	1.05	0.02	-0.08	1.06	9.88	0.017	0.96	5.87
Setup 2	1.13	0.01	-0.1	1.15	8.06	0.013	0.36	5.23
Setup 3	1.15	-0.01	-0.1	1.16	7.82	0.012	-0.47	5.14
Setup 4	1.16	-0.01	-0.1	1.17	7.5	0.012	-0.44	4.77

also an observable change in the mean values recorded with device position as can be seen comparing Setups 2 through 4. High levels of turbulence we observed in the flow impacting the front left device and appeared to be spatially variable when considering the turbulence intensities observed for turbines 1 and 2 over the four cases.

The flow impacting the downstream device does so with an average inflow angle 0 degrees, with a standard deviation of 5 degrees. The mean stream-wise and resultant flow speeds recorded show that in all cases the downstream device operates in a region of higher flow velocity than the upstream devices, which confirms that for all setups the downstream device's hub is situated in a region of accelerated flow around the two upstream devices. Considering setups 2 - 4, it can be seen that increasing the lateral separation between the upstream devices increases the acceleration in the flow as observed by the ADV. Comparing setup 1 with the other cases one can see that a significant recovery of the flow downstream of the devices 1 and 2 has occurred for this setup (at around 6.8D downstream), although the slightly higher mean velocity measured than the inlet flow velocity suggests full recovery hadn't occurred. Figure 8 shows a time-series plot of the stream-wise fluid velocity measured upstream of turbine 3, the time-series plots are supplement with histograms confirming that the measured flow data adhered approximately to a normal distribution as expected. Figure 9 shows the power spectral density calculated for each setup 1D upstream of turbine 3. The PSD were calculated as defined in 1 to 3, the overbar refers to time averaging, $R(t')$ is the auto-correlation function, $U_x(t)$ and $U_x(t-t')$ are the fluid velocity time series measured via the ADV, $\mathcal{K}$ is the wavenumber, f is frequency in Hz and E is the PSD. The power spectral density was calculated using the, Welch's algorithm [17] using windows 60 seconds in length with a 50% overlap across the 300 second time-series. The power spectra shown exhibit the expected form with a plateau at lower frequencies (the energy containing region) followed by the classic -5/3 slope indicating that the measurements captured a portion of the inertial sub-range - in relation to the Turbulent energy cascade [18]. The change in gradient around the 10-50 Hz region is likely to be a result of the filtering operations, leading to a flatting of the spectra at the highest frequencies indicating the noise floor of the instrumentation

$$E(\mathcal{K}) = \int_{-\infty}^{\infty} R(t') e^{-i\mathcal{K}t'} dt' \tag{1}$$

$$\mathcal{K} = \frac{2\pi f}{\overline{U_x(t)}} \tag{2}$$

$$R(t') = \frac{\overline{U_x(t)U_x(t-t')}}{\overline{U_x^2}} \tag{3}$$

B. Turbine Performance Analysis

In this section the power output of turbine 3 is analysed for the four differing setups to identify the effect of the array structure on the power produced by the downstream device. Figure 10 shows an example

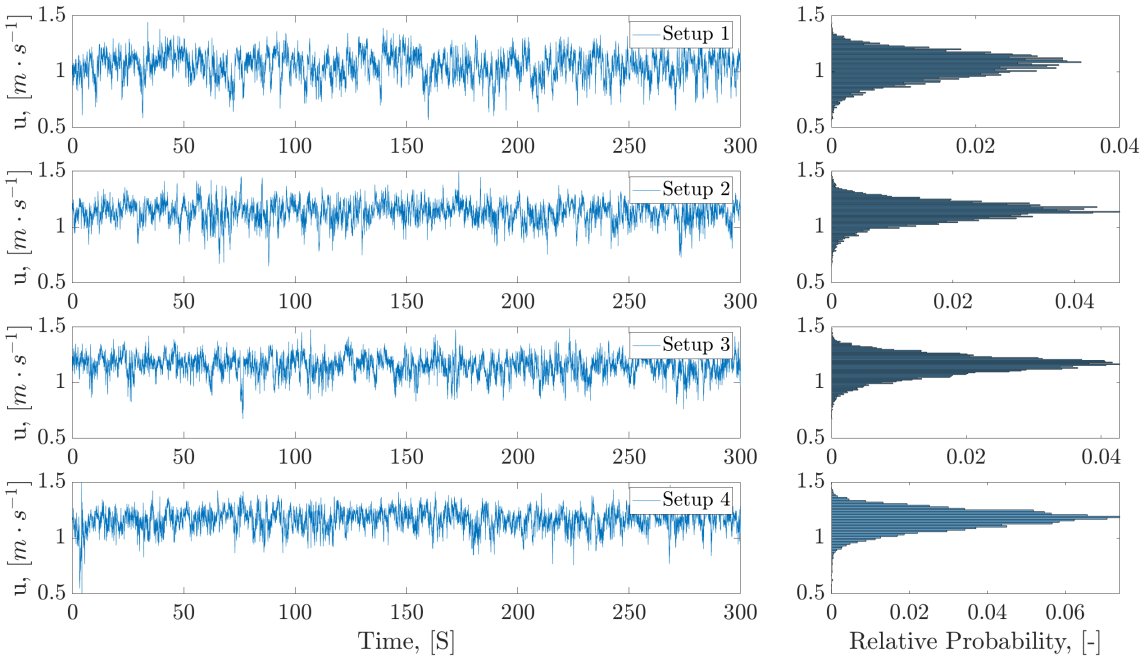

Fig. 8. Time series and histograms of the ADV measurements 1D upstream of the turbine 3 (back device) for each of the four setups.

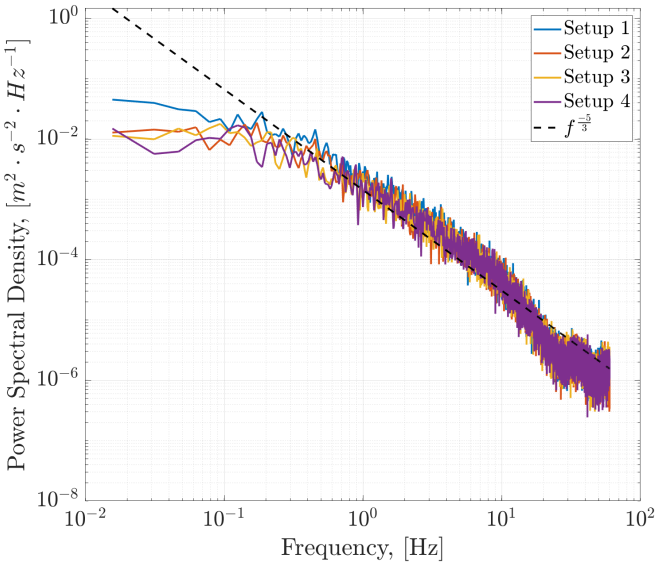

Fig. 9. Power Spectral Density of the ADV measurements 1D upstream of the turbine 3 (back device) for each of the four setups.

of the power time-series recorded during the experiments. The time-series present the electrical power developed by the PMSM housed within the device nacelle, the power is calculated by using measurements of the torque generating current or quadrature axis current, i_q which is scaled by a torque constant for the device (6.60 Nm/A), this provides a time-series of braking torque developed by the generator which is subsequently multiplied by the rotational velocity of the device, ω, in rad/s to give the power developed, as detailed in equation 4.

$$Power = 6.60 \cdot i_q \cdot \omega = \tau\omega \tag{4}$$

The results shown in Figure 10 are related to a rotational velocity of 7 rad/s and illustrates the variability of the power developed under each case whilst confirm via the supplementary histograms the roughly normal distribution of the data recorded. Under setup 2 portions of the results harboured drift in the operating rotational velocity of the device - the portions were distinct and were removed and discounted by removing all sample values where the rotational velocity was outside a 2 RPM window centred at the specified rotational velocity for the given test.

Figures 11 and 12 show heat map charts of the mean power against the setup on the x-axis and the rotational speed on the y-axis. The maximum mean power extraction was observed for setup 3 at 9.42 rad/s and the minimum mean power extraction was observed for setup 4 at 5.23 rad/s. For setup 1 peak power extraction was found at 8.34 rad/s whereas for setups 2 - 4 peak power extraction occurred at the higher rotational velocity of 9.42 rad/s. The test case showing the greatest variability in power output was observed under setup 2 at a rotational velocity of 11.5 rad/s. In the peak power extraction region, at rotational velocities above 7.4 rad/s the separation of the upstream devices seems to have had a significant effect on the power variability with setups with smaller lateral spacing (Setups 1 and 2) exhibiting higher and similar levels of power variability compared to the setups with a greater lateral separation (Setups 3 and 4). These results strongly suggest that taking advantage of the acceleration region around devices will allow for increased power production from downstream devices. Furthermore, an upstream hub to hub separation of 2.7D and greater may reduce power variability associated with such operation.

Figure 13 shows the C_p vs λ curve for the four setups and draws a comparison with previous characterisations of the device at the Kelvin Hydrodynamic Laboratory at the University of Strathclyde, full details of the testing relating to the characteristic curve can be found in [15]. Here, the λ and C_p quantities are defined

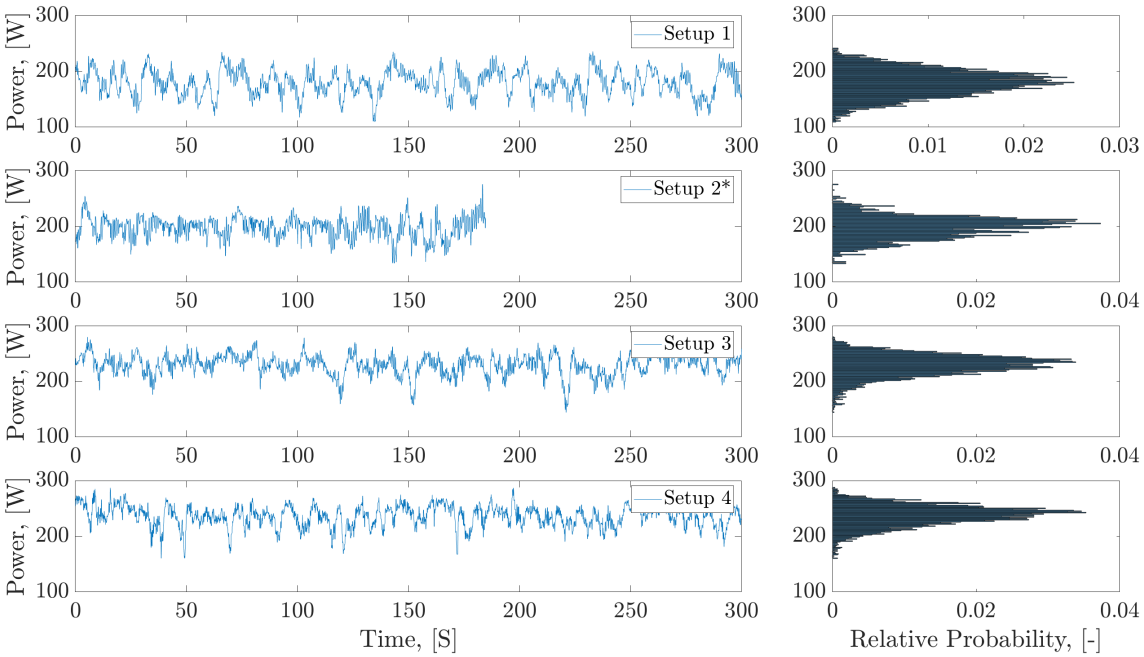

Fig. 10. Electrical power developed by turbine 3 (back device) for each of the four setups. *Due to a control error which caused momentary deviations from the set rotational velocity this test case has been filtered with such regions removed.

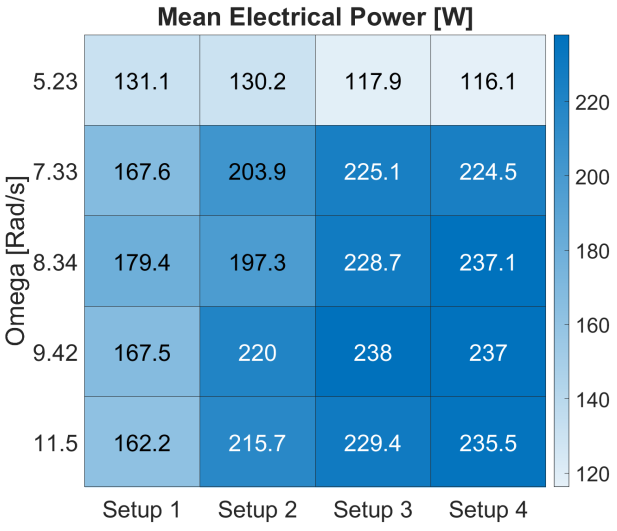

Fig. 11. Heat map of the mean electrical power developed by turbine 3 (back device) for each of the four setups and five rotational velocities tested.

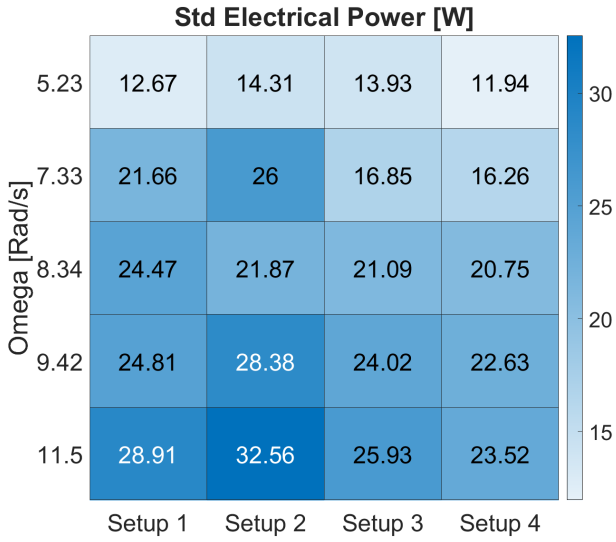

Fig. 12. Heat map of the standard deviation of the electrical power developed by turbine 3 (back device) for each of the four setups and five rotational velocities tested.

in (5) and (6), respectively - where ω is the rotational speed of the HATT rotor, τ is the torque developed by the rotor, ρ is the density of water and A is the rotor swept area.

$$\lambda = \frac{\omega \cdot r}{\overline{U_x}} \tag{5}$$

$$C_P = \frac{\omega \cdot \tau}{0.5\rho A \overline{U_x}^3} \tag{6}$$

Figure 13 shows, as error-bars, the uncertainty associated with the mean C_p vs λ and values calculated. The calculation of the uncertainty utilised the standard method of uncertainty propagation as detailed in [19]. Immediately identifiable is the discrepancy between the characteristic curve and the observations based on the current set of experiments. This discrepancy, clearly observable for $\lambda > 3$, suggests that the flow measurements taken at single point 1D upstream of the device were insufficient to adequately characterise the flow field experienced by turbine 3 and at least 5 measurements should have been made over the device swept area to fully quantify the inflow conditions. The findings would suggest that for each case a large portion of the rotor is operating in a region where the fluid velocity is greater than the mean values reported in Table VI. To gain insight in to the level this discrepancy, Figure 14 reports the flow velocity required in each case to preserve the non dimensional values of the characteristic curve. The Figure highlights that upstream flow experience by the rotor is likely to be on average between 5 and 10 % higher than the

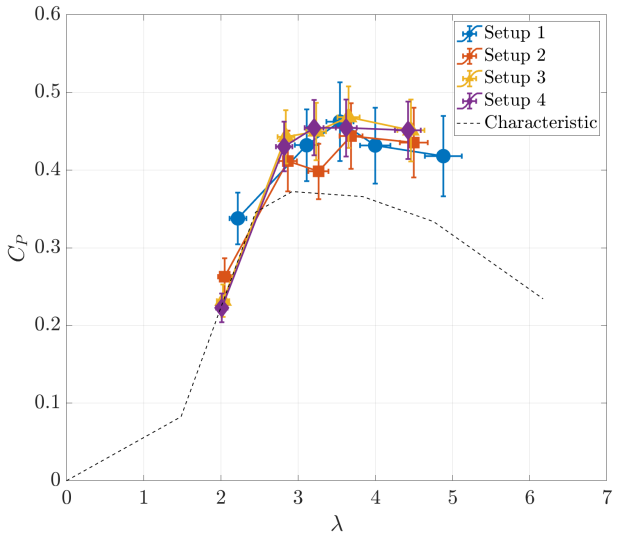

Fig. 13. Power coefficient, C_P, against tip speed ratio, λ, for each of the 4 setups with a characteristic set of values shown from previous test campaigns as detailed in [15].

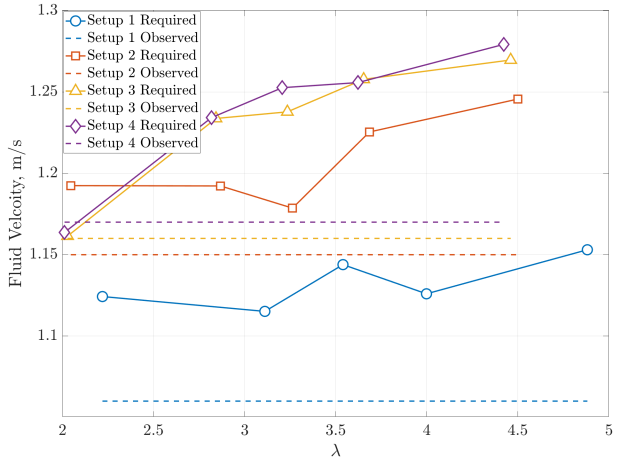

Fig. 14. Discrepancy between fluid velocities observed at the hub centre 1D upstream of turbine 3 and the fluid velocity required to meet the characteristics reported in [15]

values which in turn would result in a reduction in the λ values observed.

Finally, the transient aspects of the power production were considered in more detail by studying the spectral characteristics of the power produced under each of the four setups. Indeed this experimental data provides an opportunity to exam the spectral characteristics of power production under the differing array setups and the resulting inflow characteristics. Figure 15 shows the power spectral density of the power production time series recorded - the plots show data from the peak power extraction tests for each setup which resulted in using data for the test cases at $\omega = 8.34 rads^{-1}$ for setups 1 and 4, with data taken from test cases $\omega = 9.42 rads^{-1}$ for setups 2 and 3. The frequency axis (x-axis) has been normalised by the rotational velocity in hertz ($\frac{\omega}{2\pi}$) for each case to facilitate comparison. Furthermore, comparison curves have been plotted illustrating the $f^{-5/3}$ and $f^{-11/3}$ gradients related to the turbulent energy cascade [18] and the theoretic rotor response detailed in [20] where by the rotor

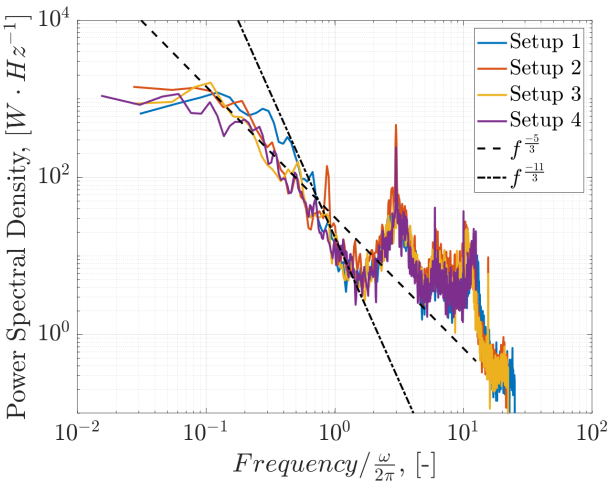

Fig. 15. Power Spectral Density of the electrical power measurements 1D upstream of the turbine 3 (back device) for each of the four setups

behaves like a low pass filter reacting more acutely to low frequency flow artefacts. The figure highlights a similar overall structure to each of the spectra plotted which is to be expected based on the commonalities in the flow spectra and rotor behaviour for each of the experiments. For the given setup the rotor obeys the $f^{-5/3}$ gradient for the initial portion of the inertial sub-range and quickly increases in steepness to follow the $f^{-11/3}$ gradient. The adherence to the steeper $f^{-11/3}$ gradient, as predicted in [20], gives way to the peaks at $\frac{2\pi f}{\omega} = 3$ for the given test, these peaks are reflected in higher harmonics at $\frac{2\pi f}{\omega} = 6$ and $\frac{2\pi f}{\omega} = 9$. Such peaks have been observed in many of the lab-scale test campaigns reported (e.g. [12] [21]) and have been modelled in the wind industry by rotational spectra [22] and more recently in the tidal application in [21]. In Figure 9 the flow spectra for Setup 1 exhibited higher energy levels in the low frequency or energy generating region - this effect is not obviously observable in Figure 15 but could account for the slight deviation from the other cases in the $10^{-1} < \frac{2\pi f}{\omega} < 1$ region. Setup 2 shows the largest amplitude peak at $\frac{2\pi f}{\omega} = 3$ which is likely to have arisen from asymmetries in the flow incoming flow due to the wakes of the upstream devices which for setup 2 had the smallest lateral separation of 2.0D. Surprisingly, setup 4 (upstream device lateral separation 3.0D) also shows a significant peak at $\frac{2\pi f}{\omega} = 3$ also which again is likely to be the result of flow asymmetries however a more detail study would be required to further understand these effects which were not observable for Setup 3.

V. Conclusion

The paper presents a results from a test campaign designed to study the effects of array layout on power production and in particular the effect of lateral spacing of upstream devices and proximity of the downstream device. The results agree with many of the findings outlined in Section II that tightly packing devices can lead to exploitation of the acceleration regions created due to the bypassed flow around upstream devices. This study in particular found that the a lateral

hub-to-hub separation of 2D negatively effects power output and variability in comparison to cases with 2.7D and 3D lateral separation - all for a longitudinal spacing of 3D. Similar power outputs we found in the 2.7D and 3D cases without significant difference in power variability. Setup 1 with greatest longitudinal spacing, 7.8D, exhibited the worst power production. In all cases spectral characteristics reported in literature were found adding to the body of evidence supporting the use of recently developed spectral models.

ACKNOWLEDGEMENT

Access:The access was supported Wave energy Scotland and UKCMER Flex Award 24835798" Funding: This work was supported by the Engineering and Physical Sciences Research Council [DyLoTTA –EP/N020782/1];Engineering and Physical Sciences Research Council[Cardiff University Impact Acceleration Account-EP/R51150X/1].

REFERENCES

[1] "Meygen — tidal projects — simec atlantis energy." [Online]. Available: https://simecatlantis.com/projects/meygen/

[2] MeygenLtd, "Lessons learnt from meygen phase 1a part 1/3: Design phase," 2017.

[3] "Nova wins €5 million european tidal energy project to slash cost of tidal energy." [Online]. Available: https://www.novainnovation.com/news/

[4] P. Mycek, B. Gaurier, G. Germain, G. Pinon, and E. Rivoalen, "Experimental study of the turbulence intensity effects on marine current turbines behaviour. part i: One single turbine," *Renewable Energy*, vol. 66, pp. 729–746, 6 2014.

[5] R. Malki, I. Masters, A. J. Williams, and T. N. Croft, "Planning tidal stream turbine array layouts using a coupled blade element momentum - computational fluid dynamics model," *Renewable Energy*, vol. 63, pp. 46–54, 3 2014.

[6] P. Stansby and T. Stallard, "Fast optimisation of tidal stream turbine positions for power generation in small arrays with low blockage based on superposition of self-similar far-wake velocity deficit profiles," *Renewable Energy*, vol. 92, pp. 366–375, 7 2016.

[7] S. W. Funke, P. E. Farrell, and M. D. Piggott, "Tidal turbine array optimisation using the adjoint approach," *Renewable Energy*, vol. 63, pp. 658–673, 3 2014.

[8] S. W. Funke, S. C. Kramer, and M. D. Piggott, "Design optimisation and resource assessment for tidal-stream renewable energy farms using a new continuous turbine approach," *Renewable Energy*, vol. 99, pp. 1046–1061, 12 2016.

[9] D. D. Apsley, T. Stallard, and P. K. Stansby, "Actuator-line cfd modelling of tidal-stream turbines in arrays," *Journal of Ocean Engineering and Marine Energy*, vol. 4, pp. 259–271, 11 2018. [Online]. Available: https://doi.org/10.1007/s40722-018-0120-3

[10] M. Shives and C. Crawford, "Tuned actuator disk approach for predicting tidal turbine performance with wake interaction," *International Journal of Marine Energy*, vol. 17, pp. 1–20, 4 2017.

[11] L. E. Myers and A. S. Bahaj, "An experimental investigation simulating flow effects in first generation marine current energy converter arrays," *Renewable Energy*, vol. 37, pp. 28–36, 1 2012.

[12] M. Allmark, R. Ellis, T. Ebdon, C. Lloyd, S. Ordonez-Sanchez, R. Martinez, A. Mason-Jones, C. Johnstone, and T. O'Doherty, "A detailed study of tidal turbine power production and dynamic loading under grid generated turbulence and turbine wake operation," *Renewable Energy*, vol. 169, pp. 1422–1439, 5 2020.

[13] T. Ebdon, M. J. Allmark, D. M. O'Doherty, A. Mason-Jones, T. O'Doherty, G. Germain, and B. Gaurier, "The impact of turbulence and turbine operating condition on the wakes of tidal turbines," *Renewable Energy*, vol. 165, pp. 96–116, 3 2021.

[14] D. R. Noble, S. Draycott, A. Nambiar, B. G. Sellar, J. Steynor, and A. Kiprakis, "Experimental assessment of flow, performance, and loads for tidal turbines in a closely-spaced array," *Energies*, vol. 13, p. 1977, 4 2020. [Online]. Available: https://www.mdpi.com/1996-1073/13/8/1977

[15] M. Allmark, R. Ellis, C. Lloyd, S. Ordonez-Sanchez, K. Johannesen, C. Byrne, C. Johnstone, T. O'Doherty, and A. Mason-Jones, "The development, design and characterisation of a scale model horizontal axis tidal turbine for dynamic load quantification," *Renewable Energy*, vol. 156, pp. 913–930, 8 2020.

[16] D. R. Sutherland, D. R. Noble, J. Steynor, T. Davey, and T. Bruce, "Characterisation of current and turbulence in the flowave ocean energy research facility," *Ocean Engineering*, vol. 139, pp. 103–115, 7 2017.

[17] M. H. Hayes, *Statistical Digital Signal Processing and Modeling*, 1st ed. USA: John Wiley amp; Sons, Inc., 1996.

[18] A. Kolmogorov, "Dissipation of energy in the locally isotropic turbulence," *Proceedings of the Royal Society of London. Series A: Mathematical and Physical Sciences*, vol. 434, pp. 15–17, 7 1991. [Online]. Available: https://royalsocietypublishing.org/

[19] P. Fornasini, *The Uncertainty in Physical Measurements*. Springer New York, 2008.

[20] N. Tobin, H. Zhu, and L. P. Chamorro, "Spectral behaviour of the turbulence-driven power fluctuations of wind turbines," *Journal of Turbulence*, vol. 16, pp. 832–846, 9 2015. [Online]. Available: http://www.tandfonline.com/doi/full/10.1080/14685248.2015.1031242

[21] G. Deskos, G. S. Payne, B. Gaurier, and M. Graham, "On the spectral behaviour of the turbulence-driven power fluctuations of horizontal-axis turbines," *Journal of Fluid Mechanics*, vol. 904, pp. 13–14, 2020. [Online]. Available: https://doi.org/10.1017/jfm.2020.681

[22] T. Burton, N. Jenkins, D. Sharpe, and E. Bossanyi, "Design loads for horizontal axis wind turbines," pp. 193–323, 5 2011. [Online]. Available: http://doi.wiley.com/10.1002/9781119992714.ch5